Journal of Applied Physics

RESEARCH ARTICLE | OCTOBER 22 2025

Hybrid surface waves at microwave frequencies in superconductor–dielectric layered structures

Montasir Qasymeh

J. Appl. Phys. 138, 163903 (2025)
https://doi.org/10.1063/5.0294042

Journal of Applied Physics
ARTICLE
pubs.aip.org/aip/jap

Hybrid surface waves at microwave frequencies in superconductor–dielectric layered structures

Cite as: J. Appl. Phys. **138**, 163903 (2025); doi: 10.1063/5.0294042
Submitted: 31 July 2025 · Accepted: 5 October 2025 ·
Published Online: 22 October 2025

Montasir Qasymeh[a)]

AFFILIATIONS

Department of Electrical and Computer Engineering, Abu Dhabi University, Abu Dhabi, P.O. Box 59911, UAE

[a)]**Also at:** Office of Research and Sponsored Programs, Provost Office, Abu Dhabi University, Abu Dhabi, P.O. Box 59911, UAE.
Author to whom correspondence should be addressed: montasir.qasymeh@adu.ac.ae

ABSTRACT

Surface waves occur at the interfaces between distinct media, with several types identified across different paradigms, including electromagnetic and mechanical surface waves. In this work, I thoroughly investigate the occurrence of microwave surface waves at the interface between superconducting and dielectric layers. I theoretically demonstrate that a hybrid surface wave, combining electromagnetic (EM) fields and supercurrent vortices, propagates along the superconductor–dielectric interface. The associated EM fields occupy the dielectric layer, satisfying Maxwell's equations, while the supercurrent vortices penetrate the superconducting layer, governed by Ampèr's and London's equations. Furthermore, I show that an extended superconductor–dielectric–superconductor (S–D–S) nanostructure can support strong nanoconfinement of these hybrid microwave surface waves, reaching spatial dimensions well below the diffraction limit. The propagating modes exhibit frequency-independent dispersion, enabling high-capacity data transmission. In addition to being intrinsically lossless, these modes can be slowed by carefully tuning the nanostructure dimensions. Importantly, our investigations reveal two key findings: (1) the divergence of the supercurrent vortices is zero, indicating no net charge (Cooper pair) transport associated with the propagating modes and (2) the energy flow of the propagating modes is carried by the associated EM fields. Hence, the proposed surface wave scheme offers a promising route for long-coherence signal transmission in superconducting circuits. I note that this paradigm of microwave surface waves has the potential to enable a new class of superconducting devices.

I. INTRODUCTION

Surface waves exist in various physical forms and have distinct applications. A prominent example is surface plasmon polaritons (SPPs), which occur at the metal–dielectric interface[1,2] and enable strong confinement below the diffraction limit in the terahertz frequency range. Several advances based on SPPs have been reported, including the merging of photonics and electronics at nanoscale dimensions,[3] sensing and detection of chemical and biological species,[4] a four-peak and high-angle tilted-insensitive surface plasmon resonance graphene absorber,[5] multifunctional metasurfaces,[6] methane concentration sensors with enhanced sensitivity,[7] liquid-analyte biosensors,[8] and ultrasensitive gas detectors,[9] to mention just a few examples. However, in the microwave frequency range, SPP waves do not naturally exist, since metals cannot support internal plasmonic oscillations at these frequencies. Nevertheless, a variety of plasmonic-inspired structures operating at microwave frequencies have been developed and experimentally demonstrated in recent years.[10] These include metallic microstructures incorporating slender wire arrays[11] and structured metal surfaces perforated with holes (supporting the so-called spoof SPPs).[12] In general, the size of these structures is on the millimeter scale, and dissipation remains a major limitation for practical applications.[13,14]

Superconductors, on the other hand, exhibit zero electrical resistance, and magnetic fields penetrate them only to limited depths.[15] This penetration is characterized by the London penetration depth, denoted λ, which is typically a few nanometers in most superconducting materials.[16] Superconductivity can be described by various theories, including the Bardeen–Cooper–Schrieffer (BCS) theory[17] and the Ginzburg–Landau theory.[18] According to BCS theory, superconductivity arises from the formation of Cooper pairs—pairs of electrons bound by an effective attractive interaction—that form a collective state known as the BCS state. These Cooper pairs enable the flow of supercurrents without resistance. Furthermore, there are characteristic length scales over which these moving pairs maintain coherence. The Ginzburg–Landau framework similarly predicts such behavior, with the coherence length ξ related to the penetration depth λ via $\xi = \kappa\lambda$. Here, κ is a dimensionless parameter known as the Ginzburg–Landau parameter, which typically satisfies $0 < \kappa < \frac{1}{\sqrt{2}}$ for type-I superconductors. Experimental characterizations of several superconducting materials have been reported,[19,20] showing that the coherence length typically ranges from hundreds to thousands of nanometers.[21] This range imposes practical limitations on applications requiring extended coherence, such as scaled quantum computers and distributed quantum signal processing.[22,23]

Surface wave propagation at microwave frequencies in layered superconductor–dielectric structures was previously investigated in Refs. 24 and 25. In Ref. 24, electromagnetic field solutions were derived by combining Maxwell's equations with London's equations and the two-fluid model, enabling a detailed analysis of transverse magnetic (TM) modes in thin-film superconducting strip transmission lines. The study established a foundational understanding of low-loss, dispersionless wave modes as a function of film geometry and penetration depth. In Ref. 25, the framework was extended through both theoretical and experimental studies, showing that the phase velocity of slow waves in superconducting thin-film lines is strongly influenced by film thickness, interfilm spacing, and the temperature-dependent penetration depth. These works were motivated by the need to provide critical insights into the temperature-dependent electrodynamics of superconducting structures and to validate theoretical predictions with experimental data.

In this work, I revisit the propagation of microwave surface waves at the interface between dielectric and superconducting layers. I demonstrate that a hybrid surface wave, composed of coupled electromagnetic fields and supercurrent vortices, exists at this interface. In this hybrid mode, the electromagnetic fields occupy the dielectric side, extending significantly into the layer in a manner reminiscent of bulk configurations, while the supercurrent vortices dominate the superconducting side, confined within the penetration depth λ, typically only a few nanometers. Our analysis shows that the energy flow of these hybrid modes relies solely on localized supercurrent loops, with no net charge (Cooper pair) transport along the propagation direction. Instead, the energy is carried by the associated electromagnetic fields. This feature suggests strong potential for signal transmission with long coherence times, as no net charge (i.e., Cooper pair superelectrons) is transported. I further investigate superconductor–dielectric–superconductor (S–D–S) structures, in which the propagating modes of these hybrid microwave surface waves exhibit frequency-independent dispersion and spatial confinement well below the diffraction limit, reaching scales of only tens of nanometers. These unique properties could open new avenues of research and enable novel applications, similar to how traditional surface plasmon polaritons revolutionized the optical domain.[26–28] For instance, harnessing this phenomenon to construct quantum devices and logic gates may introduce a new modality with unprecedented capabilities.

The remainder of this paper is organized as follows. In Sec. II, I present the theory of surface wave propagation at the superconductor–dielectric interface. Section III introduces the extended scheme of the superconductor–dielectric–superconductor configuration. The results and discussion are given in Sec. IV, and conclusions are drawn in Sec. V.

II. THEORY

Consider a layered medium composed of superconducting and dielectric materials with an interface at $y = 0$, as shown in Fig. 1. The configuration is z independent. The superconductor is characterized by $\Lambda = \frac{m^*}{n^*(q^*)}$, and the dielectric has a relative permittivity of ε_1. Here, m^*, n^*, and q^* denote the mass, density, and charge of the superelectrons, respectively.

In the superconducting layer, where $y < 0$, supercurrents and magnetic fields can physically exist. The governing equations include Ampère's law and London's second law,[29] given by $\nabla \times \vec{H} = \vec{J}$, and $\nabla \times \Lambda \vec{J} = -\mu_0 \vec{H}$, where $\Lambda = \mu_0 \lambda^2$ and μ_0 is the free-space permeability. Here, λ is the penetration depth of the magnetic field in the superconductor. These two equations yield the magnetic Helmholtz equation, given by $\nabla^2 \vec{H} + \frac{1}{\lambda^2} \vec{H} = 0$. The field solutions can be classified into a transverse magnetic (TM) mode and a transverse supercurrent (TC) mode, as detailed in Appendix A.

In the dielectric layer ($y > 0$), electric and magnetic fields may exist. The governing equations are Maxwell's equations (Ampère's law and Faraday's law): $\nabla \times \vec{E} = -\mu_1 \mu_0 \frac{\partial \vec{H}}{\partial t}$ and $\nabla \times \vec{H} = -\varepsilon_1 \varepsilon_0 \frac{\partial \vec{E}}{\partial t}$. Here, ε_1 and μ_1 are the relative permittivity and permeability, respectively. Combining these equations gives the Helmholtz equation: $\nabla^2 \vec{H} + \varepsilon_1 \mu_1 k_0^2 \vec{H} = 0$. The field solutions can be classified into transverse magnetic (TM) and transverse electric (TE) modes, as discussed in Appendix B.

A. Propagating surface mode

For propagating modes to exist, the fields in both layers must satisfy boundary conditions, including continuity of the tangential components of the electric and magnetic fields. Although static electric fields cannot exist inside superconductors, inductive electric fields governed by London's first law are generated by supercurrents. As noted above, the solutions can be grouped into TM and TE modes, with boundary conditions examined in Subsections II A 1 and II A 2.

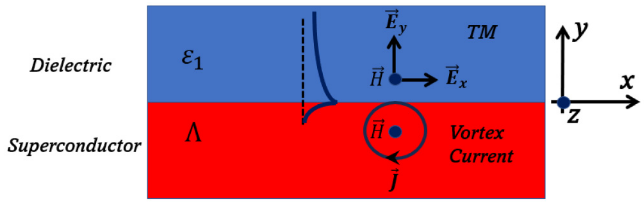

FIG. 1. A superconductor–dielectric interface. The structure is z independent. The superconductor is characterized by the parameter Λ, where the penetration depth is given by $\lambda = \sqrt{\frac{\Lambda}{\mu_0}}$, and the dielectric has a relative permittivity of ε_1.

1. Transverse magnetic mode

For transverse magnetic field distributions, the supercurrent and magnetic fields in the superconducting layer ($y < 0$) are given by (see Appendixes A and B)

$$\vec{H} = Ce^{\kappa_2 y} e^{j\beta x} e^{-j\omega t} \vec{e}_z + c.c., \tag{1}$$

$$\vec{J} = C\left(\kappa_2 \vec{e}_x - j\beta \vec{e}_y\right) e^{\kappa_2 y} e^{j\beta x} e^{-j\omega t} + c.c. \tag{2}$$

The propagation constant can be found via Ampère's and London's second equations, reading $\beta = \sqrt{\kappa_2^2 - \frac{\mu_0}{\Lambda}}$. Here, κ_2 is the transverse decay rate, C is a complex constant, $j = \sqrt{-1}$, and $c.c.$ stands for the complex conjugate.

In the dielectric layer ($y > 0$), the TM electromagnetic fields are

$$\vec{H} = Ae^{-\kappa_1 y} e^{j\beta x} e^{-j\omega t} \vec{e}_z + c.c., \tag{3}$$

$$\vec{E} = A\left(\frac{\beta}{\omega\varepsilon_0\varepsilon_1}\vec{e}_y - j\frac{\kappa_1}{\omega\varepsilon_0\varepsilon_1}\vec{e}_x\right) e^{-\kappa_1 y} e^{j\beta x} e^{-j\omega t} + c.c., \tag{4}$$

where $\beta = \sqrt{\kappa_1^2 + \varepsilon_1\mu_1 k_0^2}$ is the propagation constant, κ_1 is the transverse decay rate, and A is the complex constant.

The boundary conditions impose three relations. First, continuity of the tangential magnetic field at $y = 0$, through Eqs. (1) and (3), implies that $A = C$. Second, by calculating the inductive electric field generated by the supercurrent in the superconductor, using London's first equation $\vec{E} = \frac{\partial}{\partial t}\left(\Lambda \vec{J}\right)$, where $\vec{J}$ is the supercurrent expression in Eq. (2), and equating its tangential components to the tangential component of the electrical field in the dielectric layer in Eq. (4) at $y = 0$, one obtains the relation $\kappa_1 = \Lambda\kappa_2\omega^2\varepsilon_1\varepsilon_0$. Third, by substituting the resulting relation (i.e., $\kappa_1 = \Lambda\kappa_2\omega^2\varepsilon_1\varepsilon_0$) into the propagation constant expression $\kappa_1^2 = \beta^2 - \varepsilon_1 k_0^2$, I obtain $\Lambda^2\varepsilon_0^2\varepsilon_1^2\omega^4\kappa_2^2 = \beta^2 - \varepsilon_1 K_0^2$. Then, using $\kappa_2^2 = \beta^2 + \frac{1}{\lambda^2}$, the expression for the dispersion relation of the hybrid surface wave can be derived as

$$\beta = \sqrt{\frac{\varepsilon_1^2\lambda^2 k_0^4 + \varepsilon_1 k_0^2}{1 - \varepsilon_1^2\lambda^4 k_0^4}}, \tag{5}$$

where $k_0 = \frac{\omega}{c}$ is the free space propagation constant and c is the speed of light in free space.

For typical dielectric and superconductor parameters, the propagation constant β given by Eq. (5) is nearly equal to that of a bulk dielectric medium, $\sqrt{\varepsilon_1}k_0$. This arises because most of the surface wave energy resides in the dielectric. For example, at an air–aluminum interface (with aluminum superconducting at cryogenic temperatures, where $\lambda = 16\,\text{nm}$), and $\frac{\omega}{2\pi} = 10\,\text{GHz}$, the decay length in air is $\frac{1}{\kappa_1} = 5\,\text{cm}$, while penetration into aluminum is only $\frac{1}{\kappa_2} \approx 16\,\text{nm}$. Thus, β is almost identical to $\sqrt{\varepsilon_1}k_0$. Despite its hybrid nature, the surface wave dispersion closely resembles that of a wave in bulk dielectric. However, scenarios involving strong nanoconfinement can be realized in layered structures, as discussed in Sec. III.

2. Transverse electric mode

Field solutions with transverse supercurrent distributions in the superconducting layer are given in Eqs. (A17)–(A19), while field solutions with transverse electric distributions in the dielectric layer are given in Eqs. (B20)–(B22). Following the same procedure as above, equating tangential magnetic fields at $y = 0$, using Eqs. (B21) and (A18), $\frac{j\kappa_1}{\omega\mu_0}D = -\kappa_2\lambda^2 M$ is obtained. Second, by using London's first law with the current in Eq. (A17), and calculating the inductive electric field in the superconductor, then the continuity condition of the tangential components of two electric fields at $y = 0$ leads to $D = M\Lambda(-j\omega)$. Combining the two conditions leads to $\kappa_1 = -\kappa_2$, which implies that propagating TE hybrid surface waves cannot exist.

III. SUPERCONDUCTOR–DIELECTRIC–SUPERCONDUCTOR MULTILAYERS

Two multilayer configurations can be considered: the superconductor–dielectric–superconductor (S–D–S) and the dielectric–superconductor–dielectric (D–S–D) structures. These cases can be analyzed by extending the field expressions across the three layers and applying the boundary conditions at both interfaces. As detailed in Appendixes C and D, the D–S–D configuration provides only weak confinement, with most of the surface-wave fields residing in the dielectric layers. Therefore, this work primarily focuses on the S–D–S configuration, which exhibits strong nanoconfinement far below the diffraction limit in the microwave frequency range.

The S–D–S structure is shown in Fig. 2. The dielectric thickness is 2δ, while the superconducting layers are sufficiently thick to ensure significant decay of the supercurrent and magnetic fields along the $\pm y$ directions. By deriving the field expressions in the three layers of the S–D–S structure in the same manner as

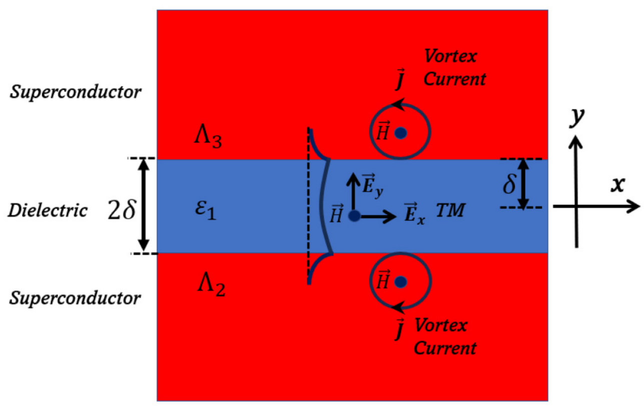

FIG. 2. A superconductor–dielectric–superconductor (S–D–S) nanostructure. The dielectric layer is centered at $y = 0$ with a width of 2δ. The superconductor layers are thick enough to ensure significant transverse decay of the supercurrent and magnetic fields along the $\pm y$ axis.

in Eqs. (1)–(4) and applying the boundary conditions at $y = \pm\delta$ (see Appendix D), the following matrix relation is obtained:

$$\begin{bmatrix} e^{2\kappa_1\delta}\left(\kappa_3\Lambda_3\omega - \frac{\kappa_1}{\omega\varepsilon_1\varepsilon_0}\right) & \kappa_3\Lambda_3\omega + \frac{\kappa_1}{\omega\varepsilon_1\varepsilon_0} \\ \kappa_2\Lambda_2\omega + \frac{\kappa_2}{\omega\varepsilon_2\varepsilon_0} & e^{2\kappa_1\delta}\left(\kappa_2\Lambda_2\omega - \frac{\kappa_1}{\omega\varepsilon_1\varepsilon_0}\right) \end{bmatrix} \begin{bmatrix} A \\ D \end{bmatrix} = \begin{bmatrix} 0 \\ 0 \end{bmatrix}. \tag{6}$$

The dispersion relation follows from the determinant condition of this matrix, yielding

$$e^{4\kappa_1\delta} = \frac{\left(\kappa_3\Lambda_3\omega + \frac{\kappa_1}{\omega\varepsilon_0\varepsilon_1}\right)}{\left(\kappa_3\Lambda_3 - \frac{\kappa_1}{\omega\varepsilon_0\varepsilon_1}\right)} \times \frac{\left(\kappa_2\Lambda_2\omega + \frac{\kappa_1}{\omega\varepsilon_0\varepsilon_1}\right)}{\left(\kappa_2\Lambda_2 - \frac{\kappa_1}{\omega\varepsilon_0\varepsilon_1}\right)}. \tag{7}$$

For a symmetric structure with $\Lambda_3 = \Lambda_2 = \Lambda$ and $\kappa_3 = \kappa_2$, the dispersion relation is given by $e^{2\kappa_1\delta} = \pm\frac{\left(\kappa_2\Lambda\omega + \frac{\kappa_1}{\omega\varepsilon_0\varepsilon_1}\right)}{\left(\kappa_2\Lambda - \frac{\kappa_1}{\omega\varepsilon_0\varepsilon_1}\right)}$. One possible solution to this relation is expressed as

$$\tanh(\kappa_1\delta) = \frac{\kappa_2\varepsilon_1\lambda^2 k_0^2}{\kappa_1}. \tag{8}$$

The alternative solution is discussed in Appendix D. Equation (8) can be simplified under two conditions: (i) $\kappa_1 \ll \frac{1}{\delta}$, achievable with a sufficiently thin dielectric layer, and (ii) $\kappa_2 \approx \frac{1}{\lambda}$, which naturally holds for superconductors due to their small penetration depths. Under these assumptions, the propagation constant can be approximated as

$$\beta = k_0\sqrt{\varepsilon_1\left(\frac{\lambda}{\delta} + 1\right)}. \tag{9}$$

The validity of this approximation is numerically investigated and confirmed in Table I in Appendix D.

IV. RESULTS AND DISCUSSION

In this section, I consider an illustrative example of an aluminum–air–aluminum (S–D–S) structure, where aluminum operates at cryogenic temperatures and exhibits superconductivity. Here, the London penetration depth of aluminum is $\lambda = 16$ nm, and the microwave frequency under consideration is $\frac{\omega}{2\pi} = 10$ GHz.

A. Dispersion relation

In Fig. 3, the propagation constant β and the transverse decay coefficient κ_1 of a propagating mode in the aluminum–air–aluminum structure are shown as functions of the thickness of the insulating layer, i.e., 2δ. First, I note that these characteristics are frequency independent as long as aluminum remains in the superconducting regime. Second, the surface wave exhibits distinct properties when the dielectric thickness is comparable to the penetration depth of the superconducting material, demonstrating nanoconfinement capabilities. However, for larger dielectric thicknesses, the propagation constant β approaches that of the bulk dielectric material, $\sqrt{\varepsilon_1}k_0$. To verify the validity of Eq. (9), I calculated κ_2 from β in Fig. 3 and confirmed Eq. (8), finding perfect agreement.

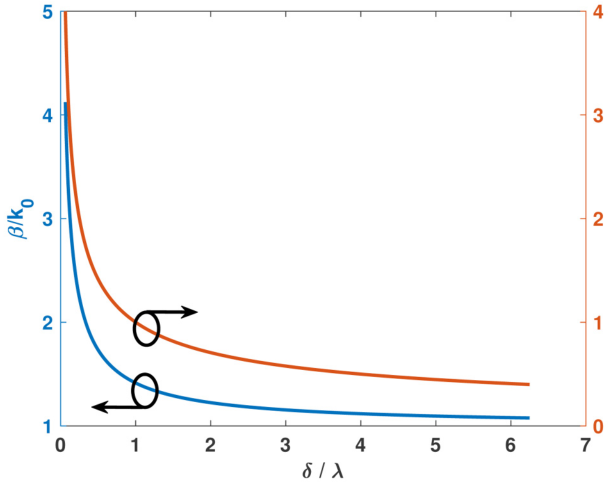

FIG. 3. Dispersion relationship of the hybrid surface wave in the Al–air–Al multilayer at cryogenic temperatures. The propagation constant β and the transverse decay rate in the dielectric layer κ_1 are shown vs δ. Here, 2δ is the thickness of the dielectric layer, $\varepsilon_1 = 1$, and $\lambda = 16$ nm is London's penetration depth for aluminum.

1. Propagation characteristics

To further investigate the surface wave properties, I calculate the group velocity and the electromagnetic wave impedance in the dielectric layer. The group velocity, defined as $v_g = \frac{\partial\omega}{\partial\beta}$, is given by

$$v_g = v_0\sqrt{\frac{\lambda}{\delta} + 1}, \tag{10}$$

where $v_0 = \frac{c}{\sqrt{\varepsilon_1}}$ is the group velocity in the bulk dielectric material. The electromagnetic wave impedance in the dielectric layer is described by $Z_{EM} = \frac{|\vec{E}|}{|\vec{H}|}$. Using the expressions in Eqs. (3) and (4), the electromagnetic wave impedance is given by

$$Z_{EM} = \frac{\beta}{\omega\varepsilon_0\varepsilon_1}\left[\left(1 - \frac{k_0^2}{\beta^2}\right)\left(1 - \frac{\tanh(\delta\kappa_1)}{\delta\kappa_1}\right) + 1\right]^{\frac{1}{2}}. \tag{11}$$

In Fig. 4, the group velocity and the electromagnetic wave impedance are presented vs δ. Here, $Z_0 = \frac{377}{\sqrt{\varepsilon_1}}$ is the electromagnetic wave impedance of the bulk dielectric.

As shown in Figs. 3 and 4, when the dielectric thickness δ increases well beyond the penetration depth λ (see Table I in Appendix D for the range of validity of the expressions), the surface wave tends to behave like a conventional electromagnetic wave propagating in the bulk dielectric medium. For instance, Eqs. (9)–(11) indicate that as $\delta \to \infty$, the propagation constant β,

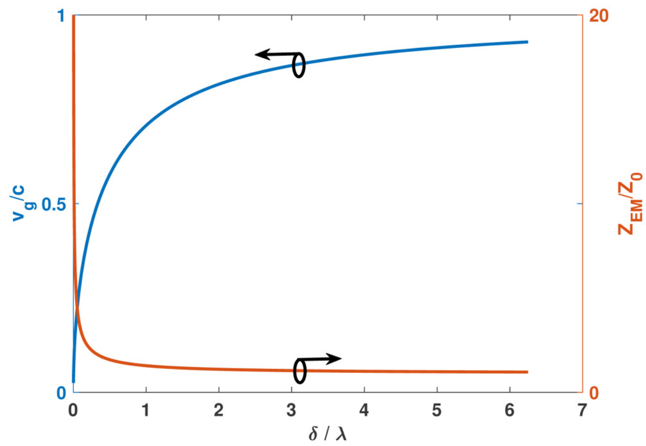

FIG. 4. The group velocity v_g and the wave impedance Z_{EM} of the propagating surface wave vs δ. Here, Z_{EM} is calculated for the associated field in the dielectric layer, $Z_0 = 377\Omega$ is the impedance of the bulk dielectric material, $\varepsilon_1 = 1$, and $\lambda = 16$ nm.

group velocity v_g, and wave impedance Z_{EM} converge to those of an EM wave in a bulk dielectric with permittivity ε_1. By contrast, when δ is comparable to λ, the wave properties are markedly different, and crucially, confinement occurs well below the diffraction limit, which cannot otherwise be achieved. Furthermore, as $\delta \to 0$, the group velocity v_g approaches zero, while the impedance Z_{EM} diverges. Hence, the most interesting regime arises when the gap thickness δ is comparable to the penetration depth λ. In this case, nanoconfinement can be achieved along with slow-wave propagation, enabling subwavelength control of microwave fields.

2. Energy flow and charge transport

A key property of the hybrid surface wave is the coupling between the supercurrent and the electromagnetic fields. To examine this behavior, I first note that the divergence of the supercurrent in Eq. (2) is zero, meaning the current forms localized loops and that no net charge (Cooper pair) transport is associated with the propagating modes. Second, I calculate the Poynting vector of the associated electromagnetic fields using Eqs. (3) and (4),

$$\hat{S} = \frac{A^2 \beta e^{-2\kappa_1 y}}{\omega \varepsilon_0 \varepsilon_1} \cos^2(\beta x - \omega t)\vec{e}_x. \tag{12}$$

These results show that the energy flow of the hybrid mode is carried by the electromagnetic fields in the dielectric layer. This is significant, as the power flow does not depend on Cooper pair transport, which typically suffers from limited coherence times. While further study is required to rigorously evaluate the coherence properties, these initial findings suggest strong potential for signal transmission in superconducting circuits with extended coherence.

V. CONCLUSION

In this work, I investigated a novel type of microwave surface wave arising at the interface between superconducting and dielectric layers. This class of surface waves consists of coupled electromagnetic (EM) fields and supercurrent vortices. The EM fields reside in the dielectric layer, while the supercurrent vortices dominate the superconducting layer. The EM fields are governed by Maxwell's equations, while the supercurrent vortices and associated magnetic fields in the superconductor satisfy both Ampère's and London's equations. The fields in both layers conform to the boundary conditions at the interface, giving rise to a propagating surface wave. Our results show that the supercurrent vortices associated with the propagating mode curl locally, while the energy flow is carried by the EM fields. This suggests the possibility of long-coherence signal transmission, offering an advantage over conventional supercurrents driven by Cooper pair transport. Furthermore, I demonstrated that a superconductor–dielectric–superconductor (S–D–S) multilayer structure enables strong confinement of these hybrid surface waves, far below the diffraction limit. Notably, the guided, nanoconfined surface wave in the S–D–S multilayer exhibits exceptional characteristics: it features frequency-independent dispersion, and its propagation speed can be precisely tuned by adjusting the dielectric thickness, enabling intentional slow-wave behavior. At the same time, it inherits the lossless nature of superconductors, offering a unique combination of tunability and near-zero dissipation. This paradigm holds great promise for advancing superconducting device design, providing a foundation for next-generation interconnects in superconducting microwave technologies.

AUTHOR DECLARATIONS

Conflict of Interest

The authors have no conflicts to disclose.

Author Contributions

Montasir Qasymeh: Conceptualization (equal); Formal analysis (equal); Investigation (equal); Methodology (equal); Validation (equal).

DATA AVAILABILITY

The data that support the findings of this study are available from the corresponding author upon reasonable request.

APPENDIX A: AMPERE'S AND LONDON'S LAWS

In a superconducting medium, the governing equations include Ampère's law and London's second equation, which can be expressed as

$$\nabla \times \overrightarrow{\mathrm{H}} = \overrightarrow{\mathrm{J}}, \tag{A1}$$

$$\nabla \times \Lambda \overrightarrow{\mathrm{J}} = -\mu_0 \overrightarrow{\mathrm{H}}, \tag{A2}$$

where $\Lambda = \mu_0 \lambda^2$, μ_0 is the free space permeability, and λ is the London's penetration depth of the superconductor material, respectively.

For a wave propagating in the x direction and independent of z, the general expressions for the magnetic field and the supercurrent can be modeled as

$$\vec{H}(x, y, z, t) = \sum_{i=x,y,z} H_i(y) e^{j\beta x} e^{-j\omega t} \hat{e}_i, \tag{A3}$$

$$\vec{J}(x, y, z, t) = \sum_{i=x,y,z} J_i(y) e^{j\beta x} e^{-j\omega t} \hat{e}_i, \tag{A4}$$

where the fields are considered z independent and $\hat{e}$ is the unit vector. The magnetic and supercurrent fields can be divided into two sets: the transverse magnetic (*TM*) mode and the transverse supercurrent (*TC*) mode.

1. TM mode

The transverse magnetic (*TM*) mode encompasses z magnetic field and a supercurrent with two x and y components with expressions that can be formulated as

$$\vec{H} = H_z(y) e^{j\beta x} e^{-j\omega t} \hat{e}_z, \tag{A5}$$

$$\vec{J} = \sum_{i=x,y} J_i(y) e^{j\beta x} e^{-j\omega t} \hat{e}_i. \tag{A6}$$

By substituting the expressions in Eqs. (A5) and (A6) in Ampere's equation in (A1), the *TM* fields obey the following relation:

$$\frac{\partial H_z}{\partial y} = J_x, \tag{A7}$$

$$\frac{\partial H_z}{\partial x} = -J_y. \tag{A8}$$

Using Ampere's and London's second equation, the governing wave equation reads

$$\frac{\partial H_z^2(y)}{\partial y^2} = \left(\beta^2 + \frac{1}{\lambda^2}\right) H_z(y). \tag{A9}$$

The solution for the field expressions satisfying Eq. (A9) can be depicted as

$$H_z = C e^{\kappa_2 y} e^{j\beta x} e^{-j\omega t}, \tag{A10}$$

$$J_x = C\kappa_2 e^{\kappa_2 y} e^{j\beta x} e^{-j\omega t}, \tag{A11}$$

$$J_y = -j\beta C e^{\kappa_2 y} e^{j\beta x} e^{-j\omega t}, \tag{A12}$$

where C is a constant and $\kappa_2 = \beta^2 + \frac{1}{\lambda^2}$.

2. TC mode

The second set is the transverse current mode (*TC*), where the magnetic field has two x and y components, while the supercurrent has only a z component. The field expressions can be presented as

$$\vec{H} = \sum_{i=x,y} H_i(y) e^{j\beta x} e^{-j\omega t} \hat{e}_i, \tag{A13}$$

$$\vec{J} = J_z(y) e^{j\beta x} e^{-j\omega t} \hat{e}_z. \tag{A14}$$

Similar to the previous case, the *TC* fields obey the following relations:

$$J_z = \frac{\partial H_y}{\partial x} - \frac{\partial H_x}{\partial y}. \tag{A15}$$

The governing wave equation, derived from Ampère's law and London's second equation, can be written as

$$\frac{\partial J_z^2(y)}{\partial y^2} = \left(\beta^2 + \frac{1}{\lambda^2}\right) J_z(y). \tag{A16}$$

The solution for field expressions is given by

$$J_z = M e^{\kappa_2 y} e^{j\beta x} e^{-j\omega t}, \tag{A17}$$

$$H_x = -\kappa_2 \lambda^2 M e^{\kappa_2 y} e^{j\beta x} e^{-j\omega t}, \tag{A18}$$

$$H_y = j\beta\lambda^2 M e^{\kappa_2 y} e^{j\beta x} e^{-j\omega t}, \tag{A19}$$

where M is a constant.

APPENDIX B: MAXWELL'S EQUATIONS

Dielectric media are governed by Maxwell's equations, which read

$$\nabla \times \vec{E} = -\mu_1 \mu_0 \frac{\partial \vec{H}}{\partial t}, \tag{B1}$$

$$\nabla \times \vec{H} = \varepsilon_1 \varepsilon_0 \frac{\partial \vec{E}}{\partial t}. \tag{B2}$$

For the considered case, the general expressions of the electric and magnetic fields can be expressed as

$$\vec{E}(x, y, t) = \sum_{i=x,y,z} E_i(y) e^{j\beta x} e^{-j\omega t} \hat{e}_i, \tag{B3}$$

$$\vec{H}(x, y, t) = \sum_{i=x,y,z} H_i(y) e^{j\beta x} e^{-j\omega t} \hat{e}_i, \tag{B4}$$

where $\hat{e}$ is the unit vector. The fields can be divided into two sets, the transverse magnetic mode, i.e., *TM*, and the transverse electric mode, i.e., *TE*.

1. TM mode

The *TM* mode includes an electric field with x and y components and a magnetic field of z component. The general field expressions can be represented as

$$\vec{E}(x, y, t) = \sum_{i=x,y} E_i(y)e^{j\beta x}e^{-j\omega t}\hat{e}_i, \tag{B5}$$

$$\vec{H}(x, y, t) = H_z(y)e^{j\beta x}e^{-j\omega t}\hat{e}_z. \tag{B6}$$

These fields satisfy the Maxwell equations, yielding the following relations:

$$j\beta E_y - \frac{\partial E_x}{\partial y} = j\omega\mu_1\mu_0 H_z, \tag{B7}$$

$$\frac{\partial E_z}{\partial y} = -j\omega\varepsilon_1\varepsilon_0 E_x, \tag{B8}$$

$$\beta H_z = -\omega\varepsilon_1\varepsilon_0 E_y. \tag{B9}$$

The governing wave equation can be obtained by combining the Maxwell equations, as follows:

$$\frac{\partial H_z^2(y)}{\partial y^2} = \left(\beta^2 - \varepsilon_1 k_0^2\right)H_z(y). \tag{B10}$$

Hence, by solving Eq. (B10), and then solving Eqs. (B7) and (B8), the solutions yield the following forms:

$$E_x = -j\frac{\kappa_1 A}{\omega\varepsilon_1\varepsilon_0}e^{-\kappa_1 y}e^{j\beta x}e^{-j\omega t}, \tag{B11}$$

$$E_y = \frac{\beta A}{\omega\varepsilon_1\varepsilon_0}e^{-\kappa_1 y}e^{j\beta x}e^{-j\omega t}, \tag{B12}$$

$$H_z = Ae^{-\kappa_1 y}e^{j\beta x}e^{-j\omega t}, \tag{B13}$$

where $\kappa_1^2 = \beta^2 - \varepsilon_1 k_0^2$ and A is a constant.

2. TE mode

The *TE* mode includes an electric field of z component and a magnetic field of x and y components, with general field expressions reading

$$\vec{E}(x, y, t) = E_z(y)e^{j\beta x}e^{-j\omega t}\hat{e}_z, \tag{B14}$$

$$\vec{H}(x, y, t) = \sum_{i=x,y} H_i(y)e^{j\beta x}e^{-j\omega t}\hat{e}_i. \tag{B15}$$

These expressions can be substituted into Maxwell's equations to result in the following relations:

$$\frac{\partial E_z}{\partial y} = j\omega\mu_0 H_x, \tag{B16}$$

$$\beta E_z = -\omega\mu_0 H_y, \tag{B17}$$

$$j\beta H_y - \frac{\partial H_x}{\partial y} = -j\omega\varepsilon_1\varepsilon_0 E_z. \tag{B18}$$

The governing wave equation in this case reads

$$\frac{\partial E_z^2(y)}{\partial y^2} = \left(\beta^2 - \varepsilon_1 k_0^2\right)E_z(y). \tag{B19}$$

Solving Eqs. (B19), (B16), and (B17) provides the following TE-mode solutions:

$$E_z = De^{-\kappa_1 y}e^{j\beta x}e^{-j\omega t}, \tag{B20}$$

$$H_x = j\frac{\kappa_1 D}{\omega\mu_0}e^{-\kappa_1 y}e^{j\beta x}e^{-j\omega t}, \tag{B21}$$

$$H_y = -\frac{\beta D}{\omega\mu_0}e^{-\kappa_1 y}e^{j\beta x}e^{-j\omega t}, \tag{B22}$$

where D is a complex constant.

APPENDIX C: MULTILAYER NANOSTRUCTURE

A layered medium can effectively manipulate the spatial confinement of propagating microwave fields. Two primary configurations can be considered: superconductor–dielectric–superconductor (S–D–S) and dielectric–superconductor–dielectric (D–S–D). The S–D–S configuration provides strong confinement, typically on the order of λ, i.e., within the nanometer scale. In contrast, in the D–S–D structure, the fields extend much more into the dielectric layers, resulting in weaker confinement. Sections 1 and 2 of Appendix C provide a detailed analysis of both configurations.

1. Superconductor–dielectric–superconductor

This section generalizes the superconductor–dielectric interface to a superconductor–dielectric–superconductor configuration, illustrated in Fig. 5. The layers are stacked along the y axis. The dielectric layer, centered at $y = 0$, has a thickness of 2δ. The superconductor layers are assumed to be much thicker than λ, ensuring sufficient field decay. The field distributions corresponding to the *TM* mode are presented in the following:

For $y > \delta$,

$$H_z = C_3 e^{-\kappa_3 y}e^{j\beta x}e^{-j\omega t}, \tag{C1}$$

$$J_x = -C_3\kappa_3 e^{-\kappa_3 y}e^{j\beta x}e^{-j\omega t}, \tag{C2}$$

$$J_y = -j\beta C_3 e^{\kappa_3 y}e^{j\beta x}e^{-j\omega t}. \tag{C3}$$

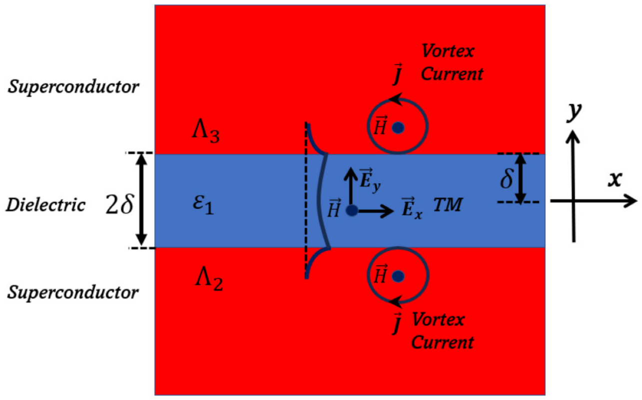

FIG. 5. A superconductor–dielectric–superconductor nanostructure.

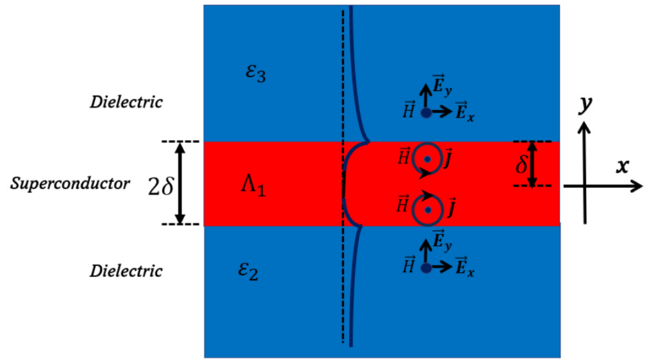

FIG. 6. A superconductor–dielectric–superconductor nanostructure.

For $-\delta > y > \delta$,

$$E_x = j\frac{\kappa_1}{\omega\varepsilon_1\varepsilon_0}Ae^{\kappa_1 y}e^{j\beta x}e^{-j\omega t} - j\frac{\kappa_1}{\omega\varepsilon_1\varepsilon_0}e^{-\kappa_1 y}e^{j\beta x}De^{-j\omega t}, \tag{C4}$$

$$E_y = \frac{\beta}{\omega\varepsilon_1\varepsilon_0}Ae^{\kappa_1 y}e^{j\beta x}e^{-j\omega t} + \frac{\beta}{\omega\varepsilon_1\varepsilon_0}De^{-\kappa_1 y}e^{j\beta x}e^{-j\omega t}, \tag{C5}$$

$$H_z = Ae^{-\kappa_1 y}e^{j\beta x}e^{-j\omega t} + De^{-\kappa_1 y}e^{j\beta x}e^{-j\omega t}. \tag{C6}$$

For $y < -\delta$,

$$H_z = C_2e^{\kappa_2 y}e^{j\beta x}e^{-j\omega t}, \tag{C7}$$

$$J_x = C_2\kappa_2e^{\kappa_2 y}e^{j\beta x}e^{-j\omega t}, \tag{C8}$$

$$J_y = -j\beta C_2e^{\kappa_2 y}e^{j\beta x}e^{-j\omega t}. \tag{C9}$$

Here, A, D, C_2, and C_3 are constants. The propagation constant is defined through the boundary conditions.

2. Dielectric-superconductor-dielectric

This section considers the D–S–D configuration shown in Fig. 6. As in the previous case, the layers are stacked along the y axis. The superconducting layer has a thickness of 2δ and is centered at $y = 0$. The insulating layers are assumed to be sufficiently thick compared to the transverse decay coefficients, i.e., κ_2 and κ_3. Under these conditions, the field distributions for the *TM* modes within the structure are obtained as follows:

For $y > \delta$,

$$E_x = -j\frac{\kappa_3}{\omega\varepsilon_3\varepsilon_0}I_3e^{-\kappa_3 y}e^{j\beta x}e^{-j\omega t}, \tag{C10}$$

$$E_y = \frac{\beta}{\omega\varepsilon_3\varepsilon_0}I_3e^{-\kappa_3 y}e^{j\beta x}e^{-j\omega t}, \tag{C11}$$

$$H_z = I_3e^{-\kappa_3 y}e^{j\beta x}e^{-j\omega t}. \tag{C12}$$

For $-\delta > y > \delta$,

$$H_z = Fe^{\kappa_1 y}e^{j\beta x}e^{-j\omega t} + Ge^{-\kappa_1 y}e^{j\beta x}e^{-j\omega t}, \tag{C13}$$

$$J_x = F\kappa_1e^{\kappa_1 y}e^{j\beta x}e^{-j\omega t} - G\kappa_1e^{-\kappa_1 y}e^{j\beta x}e^{-j\omega t}, \tag{C14}$$

$$J_y = -j\beta Fe^{\kappa_1 y}e^{j\beta x}e^{-j\omega t} - j\beta Ge^{-\kappa_1 y}e^{j\beta x}e^{-j\omega t}. \tag{C15}$$

For $y < -\delta$,

$$E_x = j\frac{\kappa_2}{\omega\varepsilon_2\varepsilon_0}I_2e^{\kappa_2 y}e^{j\beta x}e^{-j\omega t}, \tag{C16}$$

$$E_y = \frac{\beta}{\omega\varepsilon_2\varepsilon_0}I_2e^{\kappa_2 y}e^{j\beta x}e^{-j\omega t}, \tag{C17}$$

$$H_z = I_2e^{\kappa_2 y}e^{j\beta x}e^{-j\omega t}. \tag{C18}$$

Here, F, G, I_2, and I_3 are constants. The propagation contact can be defined by imposing the boundary conditions.

APPENDIX D: BOUNDARY CONDITIONS

In this section, the boundary conditions at the two interfaces of the layered structures are established, and the propagation constants of the modes are defined.

1. Superconductor–dielectric–superconductor

The boundary conditions for the S–D–S structure are as follows. At $y = \delta$: (i) continuity of the tangential magnetic field, obtained from Eqs. (C1) and (C6), and (ii) continuity of the tangential electric field, derived from Eq. (C4) together with the inductive electric field calculated via London's first equation applied to Eq. (C2). At $y = -\delta$, the same conditions apply: (1) continuity of the tangential magnetic field from Eqs. (C6) and (C7) and (2) continuity of the tangential electric field, obtained from Eq. (C14) and the electric field in Eq. (C16). These conditions lead to the following matrix formulation:

$$\begin{bmatrix} e^{2\kappa_1\delta}\left(\kappa_3\Lambda_3\omega - \frac{\kappa_1}{\omega\varepsilon_1\varepsilon_0}\right) & \kappa_3\Lambda_3\omega + \frac{\kappa_1}{\omega\varepsilon_1\varepsilon_0} \\ \kappa_2\Lambda_2\omega + \frac{\kappa_2}{\omega\varepsilon_2\varepsilon_0} & e^{2\kappa_1\delta}\left(\kappa_2\Lambda_2\omega - \frac{\kappa_1}{\omega\varepsilon_1\varepsilon_0}\right) \end{bmatrix}\begin{bmatrix} A \\ D \end{bmatrix} = \begin{bmatrix} 0 \\ 0 \end{bmatrix}. \tag{D1}$$

The dispersion relation can be calculated from the matrix in Eq. (D1) and takes the form

$$e^{4\kappa_1\delta} = \frac{\kappa_2\Lambda_2\omega + \frac{\kappa_1}{\omega\varepsilon_1\varepsilon_0}}{\kappa_2\Lambda_2\omega - \frac{\kappa_1}{\omega\varepsilon_1\varepsilon_0}} \times \frac{\kappa_3\Lambda_3\omega + \frac{\kappa_1}{\omega\varepsilon_1\varepsilon_0}}{\kappa_3\Lambda_3\omega - \frac{\kappa_1}{\omega\varepsilon_1\varepsilon_0}}. \tag{D2}$$

For symmetric superconducting layers at the two edges, in which $\Lambda_2 = \Lambda_3 = \Lambda$ and $\kappa_3 = \kappa_2$, the dispersion relation in Eq. (D2) has two solutions as in the following: One solution corresponds to the following dispersion relation:

$$\tanh(\kappa_1\delta) = \frac{\kappa_1}{\kappa_2\varepsilon_1\lambda^2 k_0^2}. \tag{D3}$$

The dispersion relation for the second solution is

$$\tanh(\kappa_1\delta) = \frac{\kappa_2\varepsilon_1\lambda^2 k_0^2}{\kappa_1}, \tag{D4}$$

where $\kappa_1^2 = \beta^2 - k_0^2\varepsilon_1$ and $\kappa_2^2 = \beta^2 + \frac{1}{\lambda^2}$.

The decay coefficient in the superconductor can be approximated as $\kappa_2 \approx \frac{1}{\lambda}$. Furthermore, assuming a thin dielectric layer such that $\delta\kappa_1 \ll 1$, Eq. (D3) admits no solution, but Eq. (D4) reduces to

$$\beta = k_0\sqrt{\varepsilon_1\left(\frac{\lambda}{\delta}+1\right)}. \tag{D5}$$

To confirm the validity of Eq. (D5), I numerically compare the value of β obtained from this approximation with the exact solution of Eq. (D4). In Table I, β is computed for various δ/λ ratios using Eq. (D5), and the corresponding values of κ_1 and κ_2 are evaluated. Substituting these values into Eq. (D4) verifies the equality of both sides, demonstrating an exact match and confirming the accuracy of the approximation.

TABLE I. Calculation of β from Eq. (D5) and verification of both sides of Eq. (D4). This table presents the computed propagation constant β as a function of normalized thickness δ/λ, including associated wave vectors κ_1 and κ_2 and the verification of Eq. (D4).

δ/λ	β (1/mm)	κ_1 (1/mm)	κ_2 (1/nm)	$\tanh(\kappa_1\delta)$	$(\kappa_2\varepsilon_1\lambda^2k_0^2)/\kappa_1$
0.1	3.35	3.33	0.0625	0.53×10^{-6}	0.53×10^{-6}
0.25	0.74	0.66	0.0625	2.67×10^{-6}	2.67×10^{-6}
0.5	0.57	0.47	0.0625	3.77×10^{-6}	3.77×10^{-6}
1	0.47	0.33	0.0625	5.33×10^{-6}	5.33×10^{-6}
2	0.40	0.23	0.0625	7.54×10^{-6}	7.54×10^{-6}
4	0.37	0.16	0.0625	10.67×10^{-6}	10.67×10^{-6}
8	0.35	0.11	0.0625	15.08×10^{-6}	15.08×10^{-6}
16	0.343	0.08	0.0625	21.33×10^{-6}	21.33×10^{-6}
24	0.34	0.06	0.0625	26.13×10^{-6}	26.13×10^{-6}
32	0.338	0.058	0.0625	30.17×10^{-6}	30.17×10^{-6}
40	0.337	0.052	0.0625	33.73×10^{-6}	33.73×10^{-6}
48	0.336	0.048	0.0625	36.95×10^{-6}	36.95×10^{-6}

2. Insulator–superconductor–insulator

I now consider the D–S–D configuration. At $y = \delta$, the boundary conditions are (1) equality of the tangential magnetic fields from Eqs. (C12) and (C13) and (2) equality of the tangential electric field from Eq. (C14) with the inductive electric field obtained from London's first equation applied to Eq. (C10). At $y = -\delta$, the conditions are (1) equality of the tangential magnetic fields from Eqs. (C13) and (C18) and (2) equality of the electric field from Eq. (C16) with the inductive electric field from Eq. (C14). These four conditions can be formulated in the following matrix:

$$\begin{bmatrix} e^{2\kappa_1\delta}\left(\frac{\kappa_3}{\omega\varepsilon_3\varepsilon_0} - \kappa_1\Lambda\omega\right) & \frac{\kappa_3}{\omega\varepsilon_3\varepsilon_0} + \kappa_1\Lambda\omega \\ \frac{\kappa_2}{\omega\varepsilon_2\varepsilon_0} + \kappa_1\Lambda\omega & e^{2\kappa_1\delta}\left(\frac{\kappa_2}{\omega\varepsilon_2\varepsilon_0} - \kappa_1\Lambda\omega\right) \end{bmatrix}\begin{bmatrix} F \\ G \end{bmatrix} = \begin{bmatrix} 0 \\ 0 \end{bmatrix}. \tag{D6}$$

The dispersion relation can be derived from Eq. (D6), given by

$$e^{4\kappa_1\delta} = \frac{\frac{\kappa_3}{\omega\varepsilon_3\varepsilon_0} + \kappa_1\Lambda\omega}{\frac{\kappa_3}{\omega\varepsilon_3\varepsilon_0} - \kappa_1\Lambda\omega} \times \frac{\frac{\kappa_2}{\omega\varepsilon_2\varepsilon_0} + \kappa_1\Lambda\omega}{\frac{\kappa_2}{\omega\varepsilon_2\varepsilon_0} - \kappa_1\Lambda\omega}. \tag{D7}$$

Again, for the case of symmetric dielectric layers at the two edges, in which $\varepsilon_2 = \varepsilon_2$ and $\kappa_3 = \kappa_2$, the dispersion relation in Eq. (D6) has two solutions. The first solution leads to the following dispersion relation:

$$\tanh(\kappa_1\delta) = \frac{\kappa_2}{\kappa_1\varepsilon_2\lambda^2 k_0^2}. \tag{D8}$$

The second solution yields the following dispersion relation:

$$\tanh(\kappa_1\delta) = \frac{\kappa_1\varepsilon_2\lambda^2 k_0^2}{\kappa_2}, \tag{D9}$$

where $\kappa_1^2 = \beta^2 + \frac{1}{\lambda^2}$ and $\kappa_2^2 = \beta^2 - k_0^2\varepsilon_2$.

As in the S–D–S case, I assume $\kappa_1 \approx \frac{1}{\lambda}$ and $\delta\kappa_1 \ll 1$. Under these assumptions, the dispersion relations yield the following solutions: Eq. (D8) gives $\kappa_2 = \varepsilon_2\lambda k_0^2\tanh(\delta/\lambda)$, while Eq. (D9) gives $\kappa_2 = \varepsilon_2\lambda k_0^2/\tanh(\delta/\lambda)$. In both cases, the confinement of the surface wave is very weak, with fields penetrating deeply into the dielectric layers—comparable to those in bulk insulating media.

For example, for a dielectric material with $\varepsilon_1 = 3.5$, the value of κ_2 is 6.2 mm in both solutions. This implies that the dielectric thickness must be at least 161.3 m to confine 63% of the field, corresponding to extremely poor confinement, essentially that of a bulk dielectric. Even with additional layering to improve confinement, the D–S–D geometry remains diffraction-limited. I, therefore, conclude that the D–S–D configuration provides substantially weaker confinement compared to the S–D–S configuration.

REFERENCES

[1] C. J. Bouwkamp, "Diffraction theory," Rep. Prog. Phys. **17**(1), 35 (1954).
[2] W. L. Barnes, A. Dereux, and T. W. Ebbesen, "Surface plasmon subwavelength optics," Nature **424**, 824–830 (2003).
[3] E. Ozbay, "Plasmonics: Merging photonics and electronics at nanoscale dimensions," Science **311**(5758), 189–193 (2006).
[4] J. Homola, "Surface plasmon resonance sensors for detection of chemical and biological species," Chem. Rev. **108**(2), 462–493 (2008).
[5] Z. Ai, H. Liu, S. Cheng, H. Zhang, Z. Yi, Q. Zeng, P. Wu, J. Zhang, C. Tang, and Z. Hao, "Four peak and high angle tilted insensitive surface plasmon resonance graphene absorber based on circular etching square window," J. Phys. D: Appl. Phys. **58**, 185305 (2025).
[6] W. Li, S. Cheng, H. Zhang, Z. Yi, B. Tang, C. Ma, P. Wu, Q. Zeng, and R. Raza, "Multi-functional metasurface: Ultra-wideband/multi-band absorption switching by adjusting guided-mode resonance and local surface plasmon resonance effects," Commun. Theor. Phys. **76**, 065701 (2024).
[7] X. Yang, Q. Song, C. Ma, Z. Yi, S. Cheng, B. Tang, C. Liu, T. Sun, and P. Wu, "A methane concentration sensor with heightened sensitivity and D-shaped cross-section U-shaped channel utilizing the principles of surface plasmon resonance," Physica E **161**, 115954 (2024).
[8] Y. Esfahani Monfared and M. Qasymeh, "Plasmonic biosensor for low-index liquid analyte detection using graphene-assisted photonic crystal fiber," Plasmonics **16**, 881–889 (2021).
[9] Y. E. Monfared and M. Qasymeh, "Graphene-assisted infrared plasmonic metamaterial absorber for gas detection," Res. Phys. **23**, 103986 (2021).
[10] F. J. Garcia-Vidal *et al.*, "Spoof surface plasmon photonics," Rev. Mod. Phys. **94**, 025004 (2022).
[11] J. B. Pendry, A. J. Holden, W. J. Stewart, and I. Youngs, "Extremely low frequency plasmons in metallic mesostructures," Phys. Rev. Lett. **76**, 4773–4776 (1996).
[12] J. B. Pendry, L. Martin-Moreeno, and F. J. Garcia-Vidal, "Mimicking surface plasmons with structured surfaces," Science **305**, 847–848 (2004).
[13] Y. J. Zhou and B. J. Yang, "Planar spoof plasmonic ultra-wideband filter based on low-loss and compact terahertz waveguide corrugated with dumbbell grooves," Appl. Opt. **54**, 4529–4533 (2015).
[14] R. Ping, H. Ma, and Y. Cai, "Compact and highly-confined spoof surface plasmon polaritons with fence-shaped grooves," Sci. Rep. **9**, 12045 (2019).
[15] W. Meissner and R. Ochsenfeld, "Ein neuer Effekt bei Eintritt der Supraleitfähigkeit," Naturwissenschaften **21**, 787–788 (1933).
[16] R. D. Parks, *Superconductivity: In Two Volumes: Volume 1* 1st ed. (CRC Press, 1969).
[17] J. Bardeen, L. N. Cooper, and J. R. Schrieffer, "Theory of superconductivity," Phys. Rev. **108**, 1175–1204 (1957).
[18] V. L. Ginzburg, "On the theory of superconductivity," Nuovo Cimento **2**, 1234–1250 (1955).
[19] J. F. Cochran and D. E. Mapother, "Superconducting transition in aluminum," Phys. Rev. **111**(1), 132–142 (1958).
[20] J. Eisenstein, "Superconducting elements," Rev. Mod. Phys. **26**(3), 277–291 (1954).
[21] M. Tinkham, *Introduction to Superconductivity* (Dover Publications, 2004), ISBN: 0486435032.
[22] M. J. Weaver, P. Duivestein, A. C. Bernasconi *et al.*, "An integrated microwave-to-optics interface for scalable quantum computing," Nat. Nanotechnol. **19**, 166–172 (2024).
[23] S. Meesala, S. Wood, D. Lake *et al.*, "Non-classical microwave-optical photon pair generation with a chip-scale transducer," Nat. Phys. **20**, 871 (2024).
[24] J. C. Swihart, "Field solution for a thin-film superconducting strip transmission line," J. Appl. Phys. **32**(3), 461–469 (1961).
[25] P. V. Mason and R. W. Gould, "Slow-wave structures utilizing superconducting thin-film transmission lines," J. Appl. Phys. **40**(5), 2039 (1969).
[26] K. L. Tsakmakidis, C. Hermann, A. Klaedtke, C. Jamois, and O. Hess, "Surface plasmon polaritons in generalized slab heterostructures with negative permittivity and permeability," Phys. Rev. B **73**(8), 085104 (2006).
[27] K. L. Tsakmakidis, A. Klaedtke, D. P. Aryal, C. Jamois, and O. Hess, "Single-mode operation in the slow-light regime using oscillatory waves in generalized left-handed heterostructures," Appl. Phys. Lett. **89**(20), 201103 (2006).
[28] K. L. Tsakmakidis, A. D. Boardman, and O. Hess, "'Trapped rainbow' storage of light in metamaterials," Nature **450**, 397–401 (2007).
[29] F. London and H. London, "The electromagnetic equations of the supraconductor," Proc. R. Soc. London A **149**, 71–88 (1935).